OIST OKINAWA INSTITUTE OF SCIENCE AND TECHNOLOGY GRADUATE UNIVERSITY
沖縄科学技術大学院大学

Biochemical characterization of the skeletal matrix of the massive coral, Porites australiensis The saccharide moieties and their localization

Author	Takeshi Takeuchi, Laurent Plasseraud, Isabelle Ziegler-Devin, Nicolas Brosse, Chuya Shinzato, Noriyuki Satoh, Frederic Marin
journal or publication title	Journal of Structural Biology
volume	203
number	3
page range	219-229
year	2018-05-30
Publisher	Elsevier
Rights	(C) 2018 Elsevier Inc.
Author's flag	author
URL	http://id.nii.ac.jp/1394/00001408/

doi: info:doi/10.1016/j.jsb.2018.05.011

Creative Commons Attribution-NonCommercial-NoDerivatives 4.0 International(https://creativecommons.org/licenses/by-nc-nd/4.0/)

Research Article

Biochemical characterization of the skeletal matrix of the massive coral, *Porites australiensis* - The saccharide moieties and their localization

Takeshi Takeuchi*[1], Laurent Plasseraud[2], Isabelle Ziegler-Devin[3], Nicolas Brosse[3], Chuya Shinzato[1,4], Noriyuki Satoh[1], and Frédéric Marin[5]

[1] Marine Genomics Unit, Okinawa Institute of Science and Technology Graduate University, Onna, Okinawa 904-0495, Japan

[2] Institut de Chimie Moléculaire de l'Université de Bourgogne, UMR CNRS 6302, Faculté des Sciences Mirande, Université de Bourgogne - Franche-Comté (UBFC), Dijon, France

[3] LERMAB, Faculté des Sciences & Technologies - Campus Aiguillettes, Université de Lorraine, Vandœuvre-Lès-Nancy, France.

[4] Department of Marine Bioscience Atmosphere and Ocean Research Institute, The University of Tokyo, Kashiwanoha, Kashiwa-shi, Chiba 277-8564, Japan

[5] UMR CNRS 6282 Biogéosciences, Bâtiment des Sciences Gabriel, Université de Bourgogne - Franche-Comté (UBFC), Dijon, France

*[*]Corresponding author**

Takeshi Takeuchi: t.takeuchi@oist.jp

© 2018. This manuscript version is made available under the CC-BY-NC-ND 4.0 license http://creativecommons.org/licenses/by-nc-nd/4.0/

27 # Abstract

28 To construct calcium carbonate skeletons of sophisticated architecture, scleractinian corals
29 secrete an extracellular skeletal organic matrix (SOM) from aboral ectodermal cells. The
30 SOM, which is composed of proteins, saccharides, and lipids, performs functions critical for
31 skeleton formation. Even though polysaccharides constitute the major component of the
32 SOM, its contribution to coral skeleton formation is poorly understood. To this end, we
33 analyzed the SOM of the massive colonial coral, *Porites australiensis*, the skeleton of which
34 has drawn great research interest because it records environmental conditions throughout the
35 life of the colony. The coral skeleton was extensively cleaned, decalcified with acetic acid,
36 and organic fractions were separated based on solubility. These fractions were analyzed using
37 various techniques, including SDS-PAGE, FT-IR, *in vitro* crystallization, CHNS analysis,
38 chromatography analysis of monosaccharide and enzyme-linked lectin assay (ELLA). We
39 confirmed the acidic nature of SOM and the presence of sulphate, which is thought to initiate
40 $CaCO_3$ crystallization. In order to analyze glycan structures, we performed ELLA on the
41 soluble SOM for the first time and found that it exhibits strong specificity to *Datura*
42 *stramonium* lectin (DSL). Furthermore, using biotinylated DSL with anti-biotin antibody
43 conjugated to nanogold, *in situ* localization of DSL-binding polysaccharides in the *P.*
44 *australiensis* skeleton was performed. Signals were distributed on the surfaces of fiber-like
45 crystals of the skeleton, suggesting that polysaccharides may modulate crystal shape. Our
46 study emphasizes the importance of sugar moieties in biomineralization of scleractinian
47 corals.

48

49

50 **Keywords**
51 *Porites australiensis*, biomineralization, coral, skeletal organic matrix, saccharide

52

53 **Abbreviations**

54 AIM: acid-insoluble matrix

55 ASM: acid-soluble matrix

56 DSL: *Datura stramonium* lectin

57 ELLA: enzyme-linked lectin assay

58 FT-IR: Fourier transform infrared spectroscopy

59 SOM: skeletal organic matrix

60

61

62 # Introduction

63 Scleractinian corals are marine animals known for their capacity to elaborate calcium
64 carbonate exoskeletons of complex shapes, many of which form reefs of great size (Spalding
65 et al., 2001). Among metazoans, scleractinians are the main producers of biogenic aragonite in
66 marine ecosystems (Milliman, 1993). From a geochemical viewpoint, scleractinian
67 biomineralization can be considered as the uptake of inorganic ions from the environment and
68 conversion of these ions into a spatially structured network of calcium carbonate biocrystals
69 that contain trace elements (Beck et al., 1992; Tambutté et al., 2011). Because this process
70 literally 'freezes' environmental information into skeletal tissues that fuel steadily
71 sedimentary archives, scleractinian skeletons are often used to reconstruct sequences of
72 paleoenvironmental conditions, in particular, past seawater temperatures via measures of
73 Sr/Ca, Li/Ca, and $\delta^{18}O$/ $\delta^{16}O$ ratios (Beck et al., 1992; Druffel, 1997; Hathorne et al., 2013;
74 Simkiss and Wilbur, 2012) or past ocean pH via boron isotopic composition ($\delta^{11}B$) (Rollion-
75 Bard et al., 2011). However, in spite of the increasing use of these geochemical proxies in
76 corals, the molecular basis of scleractinian skeleton formation is far from understood.
77
78 From a cellular viewpoint, scleractinian skeletal biomineralization is typically an epithelium-
79 driven process, *i.e.,* all precursor components of the exoskeleton are secreted by the
80 calicoblastic epithelium (also called the aboral ectoderm), a subset of the ectoderm (Allemand
81 et al., 2004; Constantz and Weiner, 1988; Tambutté et al., 2011), in contact with the nascent
82 mineral layer. These components comprise inorganic ions - calcium, bicarbonate and minor
83 elements, *i.e.*, strontium and magnesium - that are extruded via membrane channels and
84 pumps (transcellular pathway) or via intercellular space (paracellular pathway), and are
85 combined into $CaCO_3$ minerals in the sub-calicoblastic space (Tambutté et al., 2011). They
86 also include a large set of organic macromolecules that constitute the skeletal organic matrix
87 (SOM), which is allegedly released via a classical secretory pathway. This latter is however
88 poorly documented for cnidarians in general.
89
90 From a biochemical viewpoint, in many coral species examined to date, the SOM contains
91 proteins, glycoproteins, lipids, and polysaccharides that are included in the skeleton during the
92 calcification process (Constantz and Weiner, 1988; Cuif et al., 1999b; Dauphin, 2001; Farre et
93 al., 2010; Puverel et al., 2005). The SOM is distributed heterogeneously in the coral skeleton,
94 being concentrated in "centres of crystallization" (Bryan, 1941; Ogilvie, 1896) or in "early

95 mineralization zones" (Cuif et al., 2003), from which fiber-like crystals distribute radially.
96 The SOM is also detected on the top surface and growing steps in crystals (Cuif and Dauphin,
97 2005). The complex topographical relationship between the organic and mineral phases
98 suggests that the SOM plays an active role in regulating the initiation and growth of the
99 calcium carbonate crystals. In particular, the SOM contains acidic macromolecules, usually
100 considered as key-components for interacting with calcium carbonate crystals: in different *in*
101 *vitro* functional assays, they have been shown to bind calcium ions (Isa and Okazaki, 1987)
102 and modify the shapes of calcium carbonate crystal (Naggi et al., 2018; Ramos-Silva et al.,
103 2014) similarly to what has been observed with mollusc SOM (Addadi and Weiner, 1985;
104 Weiner and Hood, 1975). Amino acid analyses of SOMs of various coral species reported high
105 contents of aspartic and glutamic acids (Constantz and Weiner, 1988; Cuif et al., 1999a;
106 Gautret et al., 1997; Mitterer, 1978; Puverel et al., 2005). More recently, aspartic acid-rich
107 proteins in coral skeletons were predicted by whole genome sequencing of *Acropora*
108 *digitifera* (Shinzato et al., 2011), and subsequently confirmed by transcriptomic and
109 proteomic studies (Drake et al., 2013; Ramos-Silva et al., 2013b; Takeuchi et al., 2016).
110
111 Contrary to these recent comprehensive surveys of skeletal proteomes, sugar moieties in coral
112 SOM have not been well characterized, even though they are always detected in coral
113 skeletons and are believed to play important, although undetermined functions in
114 biomineralization (Albeck et al., 1996). The sugars in coral SOM include common
115 monosaccharides, such as neutral (fucose, rhamnose, galactose, glucose, mannose, xylose),
116 aminated (galactosamine and glucosamine) and acidic (glucuronic/galacturonic acids)
117 hexoses. Previous studies showed that their proportions vary greatly among species (Cuif et
118 al., 1999b; Naggi et al., 2018; Ramos-Silva et al., 2014), such that some present remarkable
119 monosaccharide signatures. For example, in the *Acropora millepora* SOM, arabinose
120 represents more than 60% of all monosaccharides, a finding correlated with its abundance in
121 mucus of that species (Ramos-Silva et al., 2014; Wild et al., 2005). In addition, sulphated
122 acidic sugars were detected in SOMs of several scleractinian coral species (Dauphin et al.,
123 2008; Puverel et al., 2005). However, polymeric structure and localization of saccharides in
124 coral skeletons have not been studied.
125
126 In this context, we have undertaken the overall biochemical characterization of the SOM of
127 the massive colonial coral, *Porites australiensis*. By virtue of their longevity and ability to
128 accumulate massive calcium carbonate skeletons, the genus *Porites* represents one of the most

129 important corals as a recorder of environmental conditions (Beck et al., 1992; Cobb et al., 130 2003; Linsley et al., 2000; Watanabe et al., 2011). We characterized the *Porites* SOM by using 131 various molecular analyses, including SDS-PAGE, FT-IR, CHNS analysis, and *in vitro* 132 calcium carbonate crystallization experiment. We confirmed the presence of sulphate, which 133 contributes to the acidic nature of the *Porites* SOM. Furthermore, monosaccharides were 134 quantified, and for the first time in corals, enzyme-linked lectin assay (ELLA) was performed. 135 *In situ* localization of polysaccharide in coral skeleton was achieved using a biotinylated 136 lectin (*Datura stramonium* Lectin - DSL) associated with anti-biotin antibody conjugated to 137 nanogold. Our results showed that a DSL-reactive saccharide fraction was evenly dispersed 138 on the surfaces of calcium carbonate crystals, suggesting that it may shape crystal growth 139 during coral skeleton formation.

140

141

142 Materials and methods

143 Sample collection and cleaning

144 A living coral colony of *Porites australiensis* (approx. weight 50 grams) was collected at the 145 Sesoko Marine Station, University of Ryukyus, Okinawa, Japan, under Okinawa prefecture 146 permit (Number: 20–69). The organism was immersed overnight in 3L of 10x diluted 147 household bleach solution and then extensively rinsed with water. This process, which was 148 continued until the complete removal of animal tissue and other organisms on the surface, 149 comprised the initial bleaching. The coral skeleton was rinsed, air-dried, and crushed into 150 ~2mm fragments with a Jaw-crusher (Retsch BB200). Fragments were immersed in 0.1x 151 sodium hypochlorite 10-15% (SIGMA ref. number 71696) for 50h (second bleaching). Then, 152 the fragments were washed with twice-distilled water, dried, and powdered using a mortar 153 grinder (Frisch Pulverisette 2). The powder (48 grams) was sieved (pore size <200 μm) and 154 separated into two batches. The first was subsequently decalcified (see below), while the 155 second was bleached overnight in NaOCl solution (third bleaching), thoroughly washed and 156 air-dried at 37°C before decalcification.

157

158 Extraction of skeletal organic matrices

159 The cleaned powder samples (second or third bleaching) were suspended in cold water and 160 decalcified overnight at 4°C by progressively adding (100 μL every 5 sec.) cold dilute acetic 161 acid (10% vol/vol) with an electronic burette (Titronic Universal, Schott, Mainz, Germany).

162 After 15 hours (final pH 4), the clear solution was centrifuged (3900 G, 30 min.), in order to
163 separate the pellet containing the acid-insoluble matrix or AIM from the supernatant, *i.e.*, the
164 acid-soluble matrix (ASM). The AIM pellet was resuspended in Milli-Q water, centrifuged,
165 and the supernatant discarded. After three cycles, the pellet was freeze-dried. The ASM
166 solution was filtered (5 µm) on a Nalgene filtration apparatus and concentrated by
167 ultrafiltration (Amicon stirred cell 400 mL) on a 10kDa cutoff membrane (Millipore, ref.
168 PLGC07610). The concentrated solution (15 mL) was dialyzed 4 days against 1 L MilliQ
169 water with several water changes, and freeze-dried.
170
171 **SDS-PAGE**
172 ASM lyophilisates were suspended in Milli-Q and an aliquot was added to an equal volume of
173 2x Laemmli sample buffer containing ß-mercaptoethanol. AIM pellets were gently
174 fragmented with a scalpel and a part was directly resuspended in 1x Laemmli sample buffer.
175 All preparations were denatured for 5 min at 99°C, cooled on ice and briefly centrifuged.
176 While ASM was totally dissolved by denaturation, a part of AIM remained insoluble.
177 Consequently, only the Laemmli-soluble fraction of AIM (referred to as LS-AIM) was further
178 analyzed on gels. Proteins were run on precast 10%-20% gradient mini-gels (Bio-Rad) in
179 mini-Protean III system. Gels were stained with silver nitrate (Morrissey, 1981), Stains-all
180 (Campbell et al., 1983; Marin et al., 2005) and Alcian blue (Thornton et al., 1996) at pH 1.0 in
181 order to detect sulphate groups.
182
183 **FT-IR spectroscopy**
184 FT-IR spectroscopy was used to check the overall chemical properties of the extracted
185 matrices (ASM and AIM) after two or three bleaching steps. In each case, minute chips of
186 lyophilized samples were analyzed with a Bruker Vector 22 instrument (Bruker Optics Sarl,
187 Marne la Vallée, France) fitted with a Specac Golden Gate Attenuated Total reflectance (ATR)
188 device (Specac Ltd, Orpington, UK) in the 4000–500 cm^{-1} wavenumber range (twelve scans
189 at a spectral resolution of 4 cm^{-1}). The choice for ATR mode was dictated by its reliability and
190 reproducibility, as recently shown (Beasley et al., 2014). The qualitative assignment of
191 absorption bands was performed by comparison with previously described spectra,
192 determined by us or available in the literature (Dauphin, 2001; Dauphin et al., 2008; Kanold
193 et al., 2015).
194
195 **Elemental analysis**

196 Elemental analyses were performed at the ‘‘Plateforme d’Analyse Chimique et de Synthèse
197 Moléculaire de l’Université de Bourgogne (PACSMUB)’’ on a Fisons EA 1108 CHNS-O
198 apparatus (M. Soustelle). As the technique requires 5 mg of material, only one AIM extract
199 (AIM 3bl) was tested, and the measurement was performed twice.
200
201 ***In vitro* crystallization of $CaCO_3$ with ASM**
202 *In vitro* crystal growth experiments in the presence of ASM was tested as described in a
203 previous paper (Kanold et al., 2015). In brief, 200 µL of 10 mM $CaCl_2$ containing ASM at
204 increasing concentrations (1-32 µg/ml) was applied to a 16-well culture slide (Lab-Tek,
205 Nunc/Thermo Scientific, Rochester, NY, USA). The glass slide was closed with a plastic
206 cover in which 1-mm holes were pierced above each well to allow exposure of the solution to
207 ammonium bicarbonate vapor, and sealed with Parafilm. The slide was placed in a desiccator,
208 together with ammonium bicarbonate crystals, under vacuum and incubated at 4 ˚C for 3
209 days. Subsequently, the solution was carefully removed by suction with a blunt needle
210 connected to a vacuum pump and $CaCO_3$ crystals generated on the glass bottom were dried
211 for 4h at 37˚C. These were directly observed using a tabletop scanning electron microscope
212 (TM 1000, Hitachi) without carbon sputtering.
213
214 **Monosaccharide analysis**
215 Monosaccharide quantification of ASMs and AIMs after two or three bleaching steps was
216 performed according to the HPAE-PAD technology (High Pressure Anion-Exchange - Pulsed
217 Amperometric Detection) on an ICS-3000, Dionex system equipped with a Dionex
218 CarboPac^{TM} PA-20 (3x150 mm) analytical column. In short, lyophilized samples were
219 hydrolyzed in 2M trifluoroacetic acid at 105 °C for 4 h (100 µg/100 µL), and the solution was
220 neutralized with sodium hydroxide. Hydrolytic conditions deacetylate N-acetyl-glucosamine
221 and N-acetyl-galactosamine, which are subsequently analyzed as glucosamine and
222 galactosamine, respectively. Filtered samples (20 µL) were eluted at 0.4 mL/min (35°C) using
223 the following sodium hydroxide gradient: pure water 99.2% /250 mM NaOH 0.8% : 0→20
224 min; pure water 75%/250 mM NaOH 20% /NaOAc (1M)- NaOH (20 mM) 5%: 20→37min ;
225 pure water 40% /250 mM NaOH 20%/NaOAc (1M)-NaOH (20 mM) 40%: 37→41min. Each
226 elution was followed by a wash and subsequent equilibration time. External sugar and uronic
227 acids standards were used for calibration (7 points per curve): fucose, glucose, xylose,
228 galactose, mannose, rhamnose, arabinose, glucosamine, galactosamine, galacturonic acid and
229 glucuronic acid (all provided by Sigma-Aldrich).

230

231 **Enzyme-Linked Lectin Assay (ELLA)**

232 Enzyme Linked Lectin Assay (ELLA) was conducted as described previously (Kanold et al.,
233 2015) on ASM fractions. This test, performed in solution, cannot be applied to AIM. Briefly,
234 96-well plates (MaxiSorp, Nunc/Thermo Scientific, Nunc A/S, Roskilde, Denmark) were
235 coated with ASM (50 ng/well) and incubated for 90 min at 37˚C. They were washed three
236 times with a solution of TBS/Tween-20 (0.5 mL Tween 20 per L) spread using a manual
237 microplate 8-channel washer (Nunc Immuno Wash), and subsequently blocked with Carbo-
238 free blocking solution (Vector Laboratories, ref. SP-5040) for 60 min at 37˚C. Three sets of 7
239 biotinylated lectins were tested (Vector Laboratories, Peterborough, UK, ref. BK-1000, BK-
240 2000, BK-3000). They were applied to the wells (dilution to 10 µg/mL) and incubated for 90
241 min at 37˚C. Unbound lectins were removed by washing five times with TBS/Tween-20.
242 Then, a solution containing alkaline phosphatase-conjugated avidin (Avidin-AP, Sigma
243 A7294, St Louis, MO, USA) diluted 70,000 times was added (100 µL per well) and incubated
244 for 90 min at 37 ˚C. Microplates were washed as before, and incubated with ELISA substrate
245 solution (10% vol/vol diethanolamine in Milli-Q water, pH 9.8) containing phosphatase
246 substrate (0.5 mg/mL, 4-nitrophenyl phosphate disodium salt hexahydrate (pNPP) tablet,
247 Sigma, ref. UN3500-A) at 37 °C. They were incubated at 37°C and read every 15 minutes at
248 405 nm using a Bio-Rad Model 680 micro-plate reader. Results were normalized and
249 converted to percentage of reactivity by subtracting the background (negative control
250 comprising ASM without lectin but with Avidin-AP) from all values and by considering the
251 highest response as 100%. The test was repeated at least three times. For detailed information
252 on the binding preference of each lectin, see Immel et al. (Immel et al., 2016).

253

254 ***In situ* localization: lectin-gold assay.**

255 Sodium hypochlorite-bleached fragments of *P. australiensis* skeleton were cut with a diamond
256 saw (Dremel) and one surface was flattened with fine sand paper. After rinsing with
257 sonication, the surface was finely polished with an alumine suspension (0.05 µm) on a rotary
258 polisher until a mirror polish was obtained. Samples were thoroughly cleaned by sonication
259 and submitted to bleach (NaOCl, 0.26 % active chlorine) to remove contaminants that may
260 have spread over the surface during polishing. They were rinsed twice with Milli-Q water, and
261 gently dried on Whatman paper. The flat surface was then etched 5 minutes with a solution of
262 1% EDTA (wt/vol) in the sonication bath to expose the skeletal matrix, then rinsed with Milli-
263 Q water (5 min.).

264
265 All incubation steps described after were performed at room temperature. In brief, coral
266 samples were incubated one hour in Carbo-free blocking solution alone ((Vector Laboratories,
267 ref. SP-5040), then overnight in the same solution containing the biotinylated DSL (*Datura*
268 *stramonium* lectin, diluted 100 times), and in the presence of the bactericidal agent, sodium
269 azide (0.005% wt/vol). Samples were gently rinsed several times with TBS/Tween20, then
270 incubated at least 90 minutes in a Carbo-free solution containing diluted (1/100) goat anti-
271 biotin antibody conjugated to ultra-small gold particles (0.8 nm) (GABio, Ultra Small, ref.
272 800.088; Aurion, Wareningen, The Netherlands). Samples were rinsed several times with
273 TBS/tween20 and gently dried on filter paper. Enhancement of the gold signal was achieved
274 by incubating samples in silver enhancement solution (British Biocell International, ref.
275 SEKL15) for about 15-20 minutes. Samples were rinsed once in Milli-Q water, then dried at
276 37°C.
277
278 Negative controls were performed in parallel under identical conditions, by omitting one or
279 more incubation steps: no incubation step with DSL; incubation with gold-coupled anti-biotin,
280 followed by silver enhancement; no incubation with DSL nor with biotin, but with silver
281 enhancement. All samples were carbon-sputtered and observed either with a JEOL JSM 760 F
282 field emission scanning electron microscope (JEOL, Tokyo, Japan) or with an ultra-high
283 resolution, cold-field emission Hitachi SU8230 scanning electron microscope. Quick checks
284 were performed with a tabletop SEM Hitachi TM1000. The experiment was repeated five
285 times.
286
287

288 # Results

289 **Cleaning of coral skeleton and total matrix quantification**

290 Because the *Porites* skeleton is porous, having a mesh-like structure, thorough cleaning of the
291 skeleton was required to remove soft tissues of the coral and microorganisms present in the
292 pores. We repeatedly cleaned pieces of coral skeleton by immersing them completely in
293 bleach solution and rinsing exhaustively with ultrapure water until tissue and epibionts on the
294 skeletal surface were completely removed (first bleaching). However, even though the
295 skeleton looked superficially clean after this initial treatment, a careful check using SEM
296 indicated that fibrous organic material was still present in the pores (Figure 1A, C). After a

second bleach treatment, these contaminants were removed (Figure 1B, D). Finally, to ensure the complete removal of contaminants, a third bleaching was performed on sieved skeletal powder (grain size < 200 µm). The total organic matrices were quantified after 2nd and 3rd bleaching as shown in Table 1. Interestingly, the amount of organic matrix - both soluble (ASM) and insoluble (AIM) - extracted after the 3rd bleaching was significantly lower (reduced by half) than that obtained after the 2nd one. The organic matrix represents 0.14% and 0.07% of the total skeleton by weight, after the 2nd and the 3rd bleaching, respectively.

SDS-PAGE

The ASM and the AIM (or, at least, its Laemmli-soluble moieties, referred to as LS-AIM) extracted from the 2nd and 3rd bleachings were analyzed by poly-acrylamide gel electrophoresis (SDS-PAGE) after staining with silver nitrate, Stains-all, and Alcian blue (Figure 2). Overall, broad and smeary staining was observed in all staining methods. Weak, blurred bands of high molecular weight (>170 kDa) and in the range of 50-70 kDa were detected in the silver stained gel, as well as negatively stained zones at the bottom of the lanes (<10 kDa for lane 2nd bleaching, and <17 kDa for the three other lanes) (Figure 2A). Stains-all staining showed a strong purple color in ASMs, while AIMs appeared more pinkish. (Figure 2B). Such purple staining - between metachromatic blue and red - has already been observed in a previous study for ASM of other skeletal matrices, suggesting their ability to bind calcium (Marin et al., 2005). Alcian blue staining at low-pH (pH 1.0) stained both ASM and AIM (Figure 2C), suggesting the presence of sulphate groups in all four samples (Thornton et al., 1996). Low-molecular weight ASMs stained more intensely, while for AIMS, high-molecular weight compounds stained more strongly.

FT-IR and CHNS analyses

Fourier transform infrared (FT-IR) spectra were analyzed for SOMs (Figure 3). First, the absence of the typical carbonate peaks in the ASM and in the AIM demonstrated that both extracts did not contain any contaminating salts resulting from the decalcification. In all fractions, bands attributed to protein or sugar backbones were detected at around 3380 cm^{-1}, 1650 cm^{-1}, and 1540 cm^{-1}, which correspond to amide A (νN-H), amide I (νC=O), and amide II (νC-N) bands, respectively. The signal of amide I band was stronger than that of amide II in ASM samples, while they were equivalent in AIM fractions. Weak signals at 2921-2923 cm^{-1} in AIM and 2927-2937 cm^{-1} in ASM, representing νC-H stretching vibrations, were also detected and may correspond to lipids. Signals around 1450 and 1410 cm^{-1} may be related to

331 carboxylic groups. An absorption band specific to carbohydrate was observed near 1060-1070
332 cm^{-1} in all samples. In AIM fractions, this signal was significantly weaker after the third
333 bleaching AIM with respect to the adjacent signal at 1150 cm^{-1}, which was sharply detected in
334 both AIM samples. The band at 1150 cm^{-1}, together with signals at 961, 636 and 554 cm^{-1},
335 corresponds to phosphate group (Panda et al., 2003; Rivera-Muñoz, 2011). These bands were
336 hardly visible in ASM (shoulders at 1150 cm^{-1} and 961 cm^{-1}); presumably because of their
337 weak amplitudes, they were masked by other broad signals. The signal at 1230-1250 cm^{-1} is
338 related to νS=O stretching vibration (Cabassi et al., 1978; Cael et al., 1976; Longas and
339 Breitweiser, 1991). The presence of sulfur in the third bleaching AIM was also supported by
340 CHNS analysis (Table 2).
341
342 ***In vitro* $CaCO_3$ crystallization with ASM**
343 Results of the *in vitro* crystallization assay (diffusion test) are shown in Figure 4. Crystals
344 were grown in solution containing ASM, extracted after two (Figure 4A to E) and three
345 (Figure 4G to L) bleach treatments. Addition of 1 µg/mL ASM (Figure 4A, G) resulted in
346 almost no difference with the control experiment (without ASM, Figure 4M), in which
347 typical, rhombohedral calcite crystals were synthesized. The morphology of crystals was
348 altered in the presence of 4 µg/mL ASM (Figure 4B, H). Terraced structure appeared on the
349 edges, and the crystal size was reduced. The increased concentration of ASM (16 µg/mL, 2nd
350 bleach) resulted in polycrystalline structure (Figure 4C, D), and this effect was more
351 significant at 32 µg/mL of ASM (Figure E, F). In comparison, the alteration of crystal shape
352 was more severe when high concentrations of ASM extracted after 3 bleaching steps were
353 used: at 16 µg/mL, crystal edges were rounded and the surface was rough-textured (Figure 4I,
354 J). At the highest concentration (32 µg/mL), flat crystal faces were completely destroyed, and
355 aggregation of crystals was frequently observed (Figure 4K, L). In summary, higher
356 concentrations of ASMs altered the morphology and size of $CaCO_3$ crystals, and this effect
357 was more accentuated when using ASM extracted after 3 bleaching steps.
358
359 **Monosaccharide analysis**
360 Results of the monosaccharide analysis after mild hydrolysis (with TFA) of both ASM and
361 AIM, after 2 or 3 bleaching steps, are shown in Figure 5, as relative percentages of the total
362 sugar composition. The data allow a double comparison, between AIM and ASM on the one
363 hand, and between the 2nd and 3rd bleaching on the other hand. First, in both ASMs, the most
364 abundant saccharides are galactose>arabinose>fucose, with the two first representing ≥50%

365 of all sugars. Xylose, glucosamine, glucose and mannose are minor monosaccharides
366 (between 4 and 10%) while rhamnose and galactosamine are quantitatively negligible (below
367 3%). The sugar profiles of both AIMs are somewhat similar to those of ASMs, except that
368 galactose and glucose are the dominant sugars (~≥ 20% each), with ~15% arabinose. Xylose
369 and fucose (>10%) are next most abundant, followed by glucosamine and mannose (5-10%).
370 As in ASMs, rhamnose and galactosamine are extremely minor. Galacturonic and glucuronic
371 acids were not detected in any of our samples. Second, the third bleaching treatment had a
372 more pronounced effect on ASMs than on AIMs: while it did not modify the sugar
373 abundances in AIMs, resulting in two superimposable AIM histogram patterns, it induced in
374 ASM a large decrease of arabinose (from 36.2 to 20.7%) and slight increases in galactose
375 (28.6 to 29.2%), fucose (13.2 to 16.2%), glucosamine (4.2 to 8.4%), glucose (5.1 to 7.4%) and
376 xylose (5.6 to 8.6%). However, in spite of these few percentage changes, the 3rd bleaching
377 did not fundamentally modify the monosaccharide composition pattern of ASM.
378
379 **ELLA**
380 In order to determine the types of glycan structures present in ASM (extracted after two and
381 three bleaching steps), the affinity of these two extracts for biotinylated lectins was examined
382 by enzyme-linked lectin assay (ELLA) (Kanold et al., 2015). The results, expressed as
383 percentages of reactivity with respect to the most reactive lectin, are shown in Figure 6. It is
384 noteworthy that the two ASM extracts reacted almost identically to the 21 different lectins: in
385 both cases, the strongest signal by far was observed with *Datura stramonium* lectin (DSL),
386 which preferentially binds to (β-1,4) linked GlcNAc oligomers, LacNAc, and poly-LacNAc
387 (Sondej et al., 2009). Greatly reduced affinities (20-25% of those obtained with DSL) were
388 recorded with Concanavalin A (ConA), *Lycopersicon esculentum* lectin (LEL), and *Solanum*
389 *tuberosum* lectin (STL). Other lectins including, SBA, DBA, PSA, LCA, RCA_{120}, PHA-E,
390 ECL, UEA I, SJA, PNA, Jacalin, WGA, GSL I, PHA-L, Succinylated WGA, VVA, and GSL
391 II, exhibited very weak reactivity (less than 15% of DSL) for the two ASM extracts.
392
393 ***In situ* localization study using gold-conjugated DSL**
394 Since DSL showed the strongest affinity to *Porites* ASM in ELLA, an *in situ* assay was
395 developed to localize the target saccharide moiety in the coral skeleton. Figure 7 shows SEM
396 images of the coral skeleton treated with biotinylated DSL, which was subsequently targeted
397 with an anti-biotin antibody coupled with gold nanoparticles. Figure 7A, acquired in
398 secondary electron (SE) mode, shows tips of the fibers that radiate from the early

399 mineralization zone (not shown), where crystallization occurs. Figure 7B presents the same
400 area in back-scattered electron (BSE) mode. It shows tiny bright spots that represent gold
401 particles, and consequently sugar-bound biotinylated lectins. Since an SEM image in SE
402 mode (Figure 7A) does not show any signal, this confirms that the signals detected in BSE
403 mode come from the gold particles. In Figure 7B, there is no particular concentration of gold
404 signals at the apex of the fibers, as one might have expected. Rather, the signals are dispersed
405 along the crystal surfaces.
406 Figures 7C, D and E (in BSE mode) display successive enlargements of the same area. Here
407 again, one notices that signals are homogeneously distributed on the surfaces of the fibers,
408 irrespective of the growth lines (belt-like structures) that are perpendicular to the direction of
409 crystal growth (Figure 7C and D). At high magnification (Figure 7E), the density of spots
410 reaches about 10-15 per μm^2. At very high magnification (x100 000), gold particles can be
411 measured (diameter ~ 50 nm) (Figure 7F). In none of our experiments did we detect
412 concentrations of gold spots near the centers of the spherulites, a finding that may suggest
413 that DSL-binding sugar moieties are not involved in crystal nucleation, but that they have
414 other functions related to crystal growth. Negative controls are shown on Figure 7G (SE
415 mode) and H (BSE mode). Very few signals were obtained when gold-coupled anti-biotin was
416 added to the skeleton in the absence of biotinylated DLS, confirming the low background of
417 the sample and the specificity of sugar labeling.
418
419

420 # Discussion

421 In the present study, we have characterized the skeletal organic matrix (SOM) of the massive
422 coral, *Porites australiensis,* using various biochemical techniques, including FT-IR, CHNS,
423 ELLA, gel electrophoresis, monosaccharide analysis by chromatography, and *in vitro*
424 crystallization. We have also localized sugar components directly in the coral skeleton, with a
425 technique that we adapted for the first time for corals. Our discussion focuses on three points:
426 the influence of the bleaching, the presence of sulphate and the properties of the sugar
427 moieties.
428 As discussed in one of our earlier papers (Ramos-Silva et al., 2013a), bleaching coral skeletal
429 tissues with sodium hypochlorite is crucial for obtaining a SOM free of organic contaminants,
430 namely soft tissues originating from the ectoderm, or microorganisms accumulated in skeletal
431 pores and pockets. We chose a cleaning strategy consisting of successive bleaching treatments

432 to eliminate these contaminants, and characterized the extracted SOMs (ASMs, AIMs) after
433 the second and third bleaching steps. Depending on the technique used, we found either that
434 the third bleaching did not produce any modification of the biochemical properties of the
435 SOMs, or that it induced some significant changes.
436 Among the techniques that did not detect any change, SDS-PAGE, regardless of the staining
437 used, showed smeared patterns in all SOMs, with no differences between the two ASMs and
438 the two AIMs. Similarly, ELLA on the two ASMs showed that both exhibit very similar
439 lectin-binding signatures featuring strong reactivity with DSL, moderate affinity with ConA
440 and LEL, and very low affinity with all 18 other lectins. Last, monosaccharide analyses of the
441 AIMs showed almost no differences in their composition. Taken together, these techniques
442 suggest that the third bleaching did not alter the qualitative biochemical characteristics of the
443 saccharidic moieties of the SOM.
444 However, other techniques employed in our study evidenced noticeable effects that were
445 induced by the third bleaching step. First, the SOM quantity (ASM and AIM) was reduced by
446 half. Second, FT-IR detected a decrease of the sugar peak around 1000-1050 cm^{-1} for both
447 ASM and AIM. Third, monosaccharide analysis of the ASMs showed that arabinose was
448 significantly reduced. Finally, the *in vitro* crystallization assay evidenced a noticeable
449 difference: the ASM extracted after the third bleaching induced stronger effects on crystal
450 morphologies than the ASM extracted after the second bleaching. These results suggest that
451 some sugar-containing macromolecules of the SOM (either polysaccharides or glycoproteins)
452 are peripheral to the mineral grains and destroyed by the third bleaching step, while some
453 others are protected from the harsh treatment and should be considered as 'intracrystalline', to
454 employ the old terminology of Crenshaw (Crenshaw, 1972). It is significant that the
455 'intracrystalline' ASM fraction, which is supposed to have a strong affinity for calcium
456 carbonate, induces stronger effects *in vitro* than the ASM extracted after two bleaching steps.
457 To summarize this point, we reemphasize the importance of cleaning skeletal tissues with
458 sodium hypochlorite and think that applying successive bleaching steps to the skeletal powder
459 may be an elegant manner to pre-select SOM macromolecules that have the highest affinity to
460 the mineral phase.
461
462 Our second focus is the presence of sulphate in the SOM of *Porites australiensis*,
463 demonstrated by Alcian blue staining at low pH, FT-IR, and CHNS analysis. First, Alcian
464 blue binds polyanionic groups, whatever they are, in particular those found in
465 mucopolysaccharides. At low pH (=1), Alcian blue specifically binds sulphate-containing

466 mucopolysaccharides (Thornton et al., 1996). In the present case, both ASM and LS-AIM are
467 stained, but not identically: stronger staining occurred in the lower two-thirds of the gel for
468 ASM, and the upper third for LS-AIM, indicating that the distribution of sulphate differs in
469 these two fractions. Bulk analysis by FT-IR spectroscopy confirms the presence of sulphate
470 groups, characterized by a peak in the range 1200-1250 cm^{-1}. Interestingly, pairwise
471 comparisons of sulphate peak amplitudes from the second and third bleaching steps showed
472 that the additional cleaning treatment did not degrade sulphate. This result is consistent with
473 the CHNS analysis, which unambiguously detected sulfur (>1%) in AIM after three bleaching
474 steps. Our data consequently suggest that the sulphate-containing macromolecules - likely
475 polysaccharides - are truly intracrystalline.
476 More generally, the presence of sulfur in coral skeletons is a recurrent finding that leaves the
477 question of its role open (Dauphin et al., 2008). Previous studies demonstrated that sulfur was
478 present in the SOM of *Stylophora*, *Pavona*, *Hydnophora*, and *Merulina* (Dauphin et al., 2008;
479 Puverel et al., 2005). Furthermore, sulphated sugars were found to be predominant over
480 sulfur-containing amino acids (methionine and cysteine) in ASM (Dauphin et al., 2008). As a
481 general rule, sulphated groups on sugars (ester sulphate) increase the acidic nature of the
482 SOM. They can bind calcium ions or exert an ionotropic effect by creating a very localized
483 anionic environment to concentrate calcium ions in the vicinity of the nucleation spots.
484 Sulphate is concentrated in early mineralization zones, suggesting that it may also promote
485 crystal formation (Cuif et al., 2003; Lloyd et al., 1961). Interestingly, in other calcified tissues,
486 such as nacre of the cephalopod *Nautilus pompilius*, a chemical mapping of single nacre
487 tablets showed that sulphate-containing macromolecules were localized in a central annular
488 zone in close association with carboxylate-rich macromolecules that are supposed to be the
489 calcium carbonate nucleators (Nudelman et al., 2006). This peculiar localization suggests a
490 cooperative role of both categories of macromolecules. Clearly, future work on coral
491 biomineralization should elucidate the precise function of sulphated sugars, either as Ca^{2+}
492 concentrators or as mineral nucleators.
493
494 The third focus of our discussion concerns some specific properties of the saccharidic
495 moieties of *Porites australiensis* SOM, including the lectin-binding signature, the
496 monosaccharide composition and the *in situ* localization of DSL-binding saccharide. At first,
497 the peculiar lectin-binding signature of the ASM deserves mention. Among all tested lectins,
498 DSL gave by far the strongest signal. DSL, a lectin extracted from the jimson weed, binds
499 chitotriose, chitobiose, and N-acetyl-D-glucosamine, with decreasing affinity. Its

500 carbohydrate-binding site recognizes oligomers of N-acetyl-D-glucosamine; thus, it exhibits
501 strong affinity for chitin. DSL also binds the disaccharide N-acetyllactosamine (formed from
502 the condensation of beta-galactose and N-acetyl-glucosamine) and its oligomers. It is
503 remarkable that other lectins that typically bind chitin / chitin-like motifs, such as WGA, STL,
504 or LEL give very little or no signal with the ASM of *P. australiensis*. This may suggest that
505 the saccharidic motif predominant in ASM is not N-acetyl-glucosamine, but rather N-
506 acetyllactosamine or its oligomers. This is consistent with the high amount of galactose, by
507 far the most abundant monosaccharide identified in ASM and AIM. On the other hand, none
508 of the galactose-binding lectins, such as jacalin, PNA, SBA, GSL-1, RCA, and SJA give
509 signal with *P. australiensis* ASM, but their lack of reactivity may reflect individual
510 recognition specificities for each of them, as listed by Immel and coworkers (Immel et al.,
511 2016). Beside this, additional useful structural information can be extracted from lectin
512 signature: for instance, jacalin interacts with most O-linked glycoproteins, but is unreactive
513 with ASM, while ConA, a lectin that binds mannose of N-linked glycopeptides, gives the
514 second highest signal (although moderate). This may suggest that most ASM glycoproteins of
515 *P. australiensis* skeleton are of the N-linked-type. Fucose is the third most abundant
516 monosaccharide in ASM, but UEA-1, which binds strongly to α(1,2)-linked fucose, does not
517 react. This suggests either that fucose residues present in the ASM are predominantly of the
518 α(1,3) or α(1,6)-types, or that they occupy internal positions in the saccharidic chains, or that
519 they form fucose-containing trisaccharides, a motif that inhibits UEA-1.
520 Finally, the three most abundant sugar residues of *P. australiensis* ASM, namely galactose,
521 arabinose, and fucose, represent the residues that are predominantly represented in the soluble
522 SOM of two acroporid corals, *Montipora caliculata* and *Astreopora myriophtalma* (Cuif et
523 al., 1996). Galactose and fucose are also abundant in *Heliastrea curta* and *Fungia rependa*
524 while galactose and arabinose predominate in *Acropora danae* (Cuif et al., 1996).
525 Interestingly, the monosaccharide composition of *P. australiensis* ASM is in agreement with
526 that of zooxanthellate coral ASMs in general, which was statistically distinguished from that
527 of non-zooxanthellate coral ASMs by the presence of arabinose - a monosaccharide exclusive
528 to zooxanthellate corals - the abundance of galactose, and low amounts of galactosamine and
529 glucosamine (Cuif et al., 1999b). This monosaccharide composition contrasts singularly with
530 that recently published by Naggi and coworkers (2018) who identified by other techniques
531 (chromatography and mass spectrometry) glucuronic acid as the main saccharide residue
532 present in the SOM of three stony corals, *Astroides calycularis*, *Balanophyllia europaea*, and
533 *Stylophora pistillata*. We did not detect this acidic sugar in our samples and then reason of the

534 discrepancy between our data and theirs is not known.
535 Last, using gold-conjugated DSL, we localized sugar components that have a strong affinity
536 to DSL lectin. In all experiments, we obtained a homogeneous distribution of gold particles on
537 the surface of radiating aragonite fibers. We did not observe signals concentrated along
538 growth lines, perpendicular to fiber elongation nor signals at the tips of the fibers. Finally, the
539 centers of spherulites are enriched in organics that are supposed to be the nucleating
540 macromolecules. However, we did not detect any high concentration of gold spots around
541 these centers, *i.e.,* at the bases of the fibers that are the closest to the center. In this latter case,
542 we cannot exclude that the treatment of the polished surface - prior to lectin incubation -
543 which consists in cleaning with bleach followed by slight etching with EDTA, may have
544 eliminated most of the organics located at the centers of spherulites. In spite of these potential
545 preparation artifacts, our observations suggest that the DSL-binding saccharide fraction is
546 neither involved in crystal nucleation nor in stopping crystal growth (where it would be
547 distributed along the growth lines). Because the signal homogeneously covers the aragonite
548 fibers, and because DSL-reactive ASM exerts a significant *in vitro* effect on crystal size and
549 shape, we put forward the hypothesis that this fraction modulates size, shape, and/or fiber
550 growth kinetics. In order to better understand the role of these sugar moieties in *P.*
551 *australiensis* biomineralization, further experiments, such as *in vitro* crystallization
552 experiments with purified DSL-binding polysaccharide, should be conducted.
553

554 # Conclusions

555 Our study represents the first biochemical characterization of the skeletal organic matrix of
556 the massive coral, *Porites australiensis*, under different cleaning conditions. We focused on
557 the sugar moieties. Besides obtaining peculiar signatures of monosaccharide composition and
558 of lectin profile, we localized *in situ*, for the first time, a DSL lectin-binding fraction. Our
559 results re-emphasize the role of saccharides in coral biomineralization and aims at identifying
560 sugar signatures of coral SOMs, by waiting for understanding the structure-function
561 relationships of this class of macromolecules in biomineralization. Further investigation of
562 this organic fraction, together with the ongoing proteomic analysis of *Porites* SOM, is
563 essential to obtain the most complete picture of macromolecular constituents required for
564 building the skeleton of these major reef-forming corals.
565
566

567

568 ## Acknowledgements

569 We thank Dr. Akira Iguchi (Okinawa National College of Technology) for providing coral
570 specimens. We also thank Marcel Soustelle (PACSMUB, Dijon) for elemental analysis and
571 Frédéric Herbst for helping in handling the two SEM. We thank Dr. Steven D. Aird for editing
572 the manuscript. All data were generated during a six-month stay of Dr. T. Takeuchi (Oct.
573 2015-March 2016) in the laboratory of Dr. F. Marin, UMR CNRS 6282 Biogéosciences in
574 Dijon (UBFC).

575

576 ## Funding

577 This study was supported by internal funds from the Okinawa Institute of Science and
578 Technology (OIST).

579

580

581 # References

582 Addadi, L., Weiner, S., 1985. Interactions between acidic proteins and crystals:
583 stereochemical requirements in biomineralization. Proc. Natl. Acad. Sci. U. S. A. 82,
584 4110-4114.
585 Albeck, S., Weiner, S., Addadi, L., 1996. Polysaccharides of Intracrystalline Glycoproteins
586 Modulate Calcite Crystal Growth In Vitro. Chemistry – A European Journal 2, 278-
587 284.
588 Allemand, D., Ferrier-Pagès, C., Furla, P., Houlbrèque, F., Puverel, S., Reynaud, S., Tambutté,
589 É., Tambutté, S., Zoccola, D., 2004. Biomineralisation in reef-building corals: from
590 molecular mechanisms to environmental control. Comptes Rendus Palevol 3, 453-467.
591 Beasley, M.M., Bartelink, E.J., Taylor, L., Miller, R.M., 2014. Comparison of transmission
592 FTIR, ATR, and DRIFT spectra: implications for assessment of bone bioapatite
593 diagenesis. J. Archaeol. Sci 46, 16-22.
594 Beck, J.W., Edwards, R.L., Ito, E., Taylor, F.W., Recy, J., Rougerie, F., Joannot, P., Henin, C.,
595 1992. Sea-Surface Temperature from Coral Skeletal Strontium/Calcium Ratios.
596 Science 257, 644-647.
597 Bryan, W.H., D, 1941. Spherulitic crystallization as a mechanism of skeletal growth in the
598 hexacorals. Proceedings of Royal Society of Queensland 52, 78-91.
599 Cabassi, F., Casu, B., Perlin, A.S., 1978. Infrared absorption and raman scattering of sulfate
600 groups of heparin and related glycosaminoglycans in aqueous solution. Carbohydr.
601 Res. 63, 1-11.
602 Cael, J.J., Isaac, D.H., Blackwell, J., Koenig, J.L., Atkins, E.D.T., Sheehan, J.K., 1976.
603 Polarized infrared spectra of crystalline glycosaminoglycans. Carbohydr. Res. 50, 169-
604 179.
605 Campbell, K., MacLennan, D., Jorgensen, A., 1983. Staining of the Ca2+-binding proteins,
606 calsequestrin, calmodulin, troponin C, and S-100, with the cationic carbocyanine dye"
607 Stains-all". J. Biol. Chem. 258, 11267-11273.
608 Cobb, K.M., Charles, C.D., Cheng, H., Edwards, R.L., 2003. El Nino/Southern Oscillation
609 and tropical Pacific climate during the last millennium. Nature 424, 271-276.
610 Constantz, B., Weiner, S., 1988. Acidic macromolecules associated with the mineral phase of
611 scleractinian coral skeletons. J. Exp. Zool. 248, 253-258.
612 Crenshaw, M.A., 1972. The soluble matrix from Mercenaria mercenaria shell.
613 Biomineralization 6, 6-11.

614 Cuif, J., Dauphin, Y., Denis, A., Gautret, P., Marin, F., 1996. The organo-mineral structure of
615 coral skeletons: a potential source of new criteria for Scleractinian taxonomy. Bull.
616 Institut Océanogr. Monaco, Numéro Spécial 14, 4, 359-367.
617 Cuif, J.-P., Dauphin, Y., 2005. The two-step mode of growth in the scleractinian coral
618 skeletons from the micrometre to the overall scale. J. Struct. Biol. 150, 319-331.
619 Cuif, J.-P., Dauphin, Y., Gautret, P., 1999a. Compositional diversity of soluble mineralizing
620 matrices in some recent coral skeletons compared to fine-scale growth structures of
621 fibres: discussion of consequences for biomineralization and diagenesis. International
622 Journal of Earth Sciences 88, 582-592.
623 Cuif, J.-P., Dauphin, Y., Freiwald, A., Gautret, P., Zibrowius, H., 1999b. Biochemical markers
624 of zooxanthellae symbiosis in soluble matrices of skeleton of 24 Scleractinia species.
625 Comparative Biochemistry and Physiology Part A: Molecular & Integrative
626 Physiology 123, 269-278.
627 Cuif, J.P., Dauphin, Y., Doucet, J., Salome, M., Susini, J., 2003. XANES mapping of organic
628 sulfate in three scleractinian coral skeletons. Geochim. Cosmochim. Acta 67, 75-83.
629 Dauphin, Y., 2001. Comparative studies of skeletal soluble matrices from some Scleractinian
630 corals and Molluscs. Int. J. Biol. Macromol. 28, 293-304.
631 Dauphin, Y., Cuif, J.-P., Williams, C.T., 2008. Soluble organic matrices of aragonitic skeletons
632 of Merulinidae (Cnidaria, Anthozoa). Comparative Biochemistry and Physiology Part
633 B: Biochemistry and Molecular Biology 150, 10-22.
634 Drake, J.L., Mass, T., Haramaty, L., Zelzion, E., Bhattacharya, D., Falkowski, P.G., 2013.
635 Proteomic analysis of skeletal organic matrix from the stony coral *Stylophora*
636 *pistillata*. Proc. Natl. Acad. Sci. U. S. A. 110, 3788-3793.
637 Druffel, E.R.M., 1997. Geochemistry of corals: Proxies of past ocean chemistry, ocean
638 circulation, and climate. Proc. Natl. Acad. Sci. U. S. A. 94, 8354-8361.
639 Farre, B., Cuif, J.-P., Dauphin, Y., 2010. Occurrence and diversity of lipids in modern coral
640 skeletons. Zoology 113, 250-257.
641 Gautret, P., Cuif, J.P., Freiwald, A., 1997. Composition of soluble mineralizing matrices in
642 zooxanthellate and non-zooxanthellate scleractinian corals: Biochemical assessment of
643 photosynthetic metabolism through the study of a skeletal feature. Facies 36, 189-194.
644 Hathorne Ed, C., Felis, T., Suzuki, A., Kawahata, H., Cabioch, G., 2013. Lithium in the
645 aragonite skeletons of massive *Porites* corals: A new tool to reconstruct tropical sea
646 surface temperatures. Paleoceanography 28, 143-152.
647 Immel, F., Broussard, C., Catherinet, B., Plasseraud, L., Alcaraz, G., Bundeleva, I., Marin, F.,

648 2016. The shell of the invasive bivalve species *Dreissena polymorpha*: biochemical,
649 elemental and textural investigations. PLoS One 11, e0154264.
650 Isa, Y., Okazaki, M., 1987. Some observations on the Ca^{2+}-binding phospholipids from
651 scleractinian coral skeletons. Comp. Biochem. Physiol. B 87, 507-512.
652 Kanold, J.M., Guichard, N., Immel, F., Plasseraud, L., Corneillat, M., Alcaraz, G., Brümmer,
653 F., Marin, F., 2015. Spine and test skeletal matrices of the Mediterranean sea urchin
654 *Arbacia lixula* – a comparative characterization of their sugar signature. FEBS Journal
655 282, 1891-1905.
656 Linsley, B.K., Wellington, G.M., Schrag, D.P., 2000. Decadal Sea Surface Temperature
657 Variability in the Subtropical South Pacific from 1726 to 1997 A.D. Science 290,
658 1145-1148.
659 Lloyd, A.G., Dodgson, K.S., Price, R.G., Rose, F.A., 1961. I. Polysaccharide sulphates.
660 Biochim. Biophys. Acta 46, 108-115.
661 Longas, M.O., Breitweiser, K.O., 1991. Sulfate composition of glycosaminoglycans
662 determined by infrared spectroscopy. Anal. Biochem. 192, 193-196.
663 Marin, F., Amons, R., Guichard, N., Stigter, M., Hecker, A., Luquet, G., Layrolle, P., Alcaraz,
664 G., Riondet, C., Westbroek, P., 2005. Caspartin and Calprismin, two proteins of the
665 shell calcitic prisms of the Mediterranean fan mussel *Pinna nobilis*. J. Biol. Chem.
666 280, 33895-33908.
667 Milliman, J.D., 1993. Production and accumulation of calcium carbonate in the ocean: budget
668 of a nonsteady state. Global Biogeochemical Cycles 7, 927-957.
669 Mitterer, R.M., 1978. Amino-acid composition and metal-binding capability of skeletal
670 protein of corals. Bull. Mar. Sci. 28, 173-180.
671 Morrissey, J.H., 1981. Silver stain for proteins in polyacrylamide gels: A modified procedure
672 with enhanced uniform sensitivity. Anal. Biochem. 117, 307-310.
673 Naggi, A., Torri, G., Iacomi, M., Colombo Castelli, G., Reggi, M., Fermani, S., Dubinsky, Z.,
674 Goffredo, S., Falini, G., 2018. Structure and function of stony coral intraskeletal
675 polysaccharides. ACS Omega 3, 2895-2901.
676 Nudelman, F., Gotliv, B.A., Addadi, L., Weiner, S., 2006. Mollusk shell formation: Mapping
677 the distribution of organic matrix components underlying a single aragonitic tablet in
678 nacre. J. Struct. Biol. 153, 176-187.
679 Ogilvie, M.M., 1896. Microscopic and systematic study of madreporarian types of corals.
680 Philos. Trans. R. Soc. Lond. B Biol. Sci. 187, 83-345.
681 Panda, R.N., Hsieh, M.F., Chung, R.J., Chin, T.S., 2003. FTIR, XRD, SEM and solid state

682 NMR investigations of carbonate-containing hydroxyapatite nano-particles
683 synthesized by hydroxide-gel technique. J. Phys. Chem. Solids 64, 193-199.
684 Puverel, S., Tambutte, E., Pererra-Mouries, L., Zoccola, D., Allemand, D., Tambutte, S., 2005.
685 Soluble organic matrix of two Scleractinian corals: Partial and comparative analysis.
686 Comparative Biochemistry and Physiology B-Biochemistry & Molecular Biology 141,
687 480-487.
688 Ramos-Silva, P., Marin, F., Kaandorp, J., Marie, B., 2013a. Biomineralization toolkit: The
689 importance of sample cleaning prior to the characterization of biomineral proteomes.
690 Proc. Natl. Acad. Sci. U. S. A. 110, E2144-E2146.
691 Ramos-Silva, P., Kaandorp, J., Huisman, L., Marie, B., Zanella-Cleon, I., Guichard, N.,
692 Miller, D.J., Marin, F., 2013b. The skeletal proteome of the coral *Acropora millepora*:
693 the evolution of calcification by co-option and domain shuffling. Mol. Biol. Evol. 30,
694 2099-2112.
695 Ramos-Silva, P., Kaandorp, J., Herbst, F., Plasseraud, L., Alcaraz, G., Stern, C., Corneillat,
696 M., Guichard, N., Durlet, C., Luquet, G., Marin, F., 2014. The Skeleton of the
697 Staghorn Coral *Acropora millepora*: Molecular and Structural Characterization. PLoS
698 One 9, e97454.
699 Rivera-Muñoz, E.M., 2011. Hydroxyapatite-Based Materials: Synthesis and Characterization,
700 p. Ch. 04, in: R. Fazel-Rezai, (Ed.), Biomedical Engineering - Frontiers and
701 Challenges, InTech, Rijeka.
702 Rollion-Bard, C., Blamart, D., Trebosc, J., Tricot, G., Mussi, A., Cuif, J.-P., 2011. Boron
703 isotopes as pH proxy: A new look at boron speciation in deep-sea corals using 11B
704 MAS NMR and EELS. Geochim. Cosmochim. Acta 75, 1003-1012.
705 Shinzato, C., Shoguchi, E., Kawashima, T., Hamada, M., Hisata, K., Tanaka, M., Fujie, M.,
706 Fujiwara, M., Koyanagi, R., Ikuta, T., Fujiyama, A., Miller, D.J., Satoh, N., 2011.
707 Using the *Acropora digitifera* genome to understand coral responses to environmental
708 change. Nature 476, 320-U382.
709 Simkiss, K., Wilbur, K.M., 2012. Biomineralization Elsevier.
710 Sondej, M., Denny, P.A., Xie, Y., Ramachandran, P., Si, Y., Takashima, J., Shi, W., Wong,
711 D.T., Loo, J.A., Denny, P.C., 2009. Glycoprofiling of the Human Salivary Proteome.
712 Clin. Proteomics 5, 52-68.
713 Spalding, M., Ravilious, C., Green, E.P., 2001. World atlas of coral reefs Univ of California
714 Press.
715 Takeuchi, T., Yamada, L., Shinzato, C., Sawada, H., Satoh, N., 2016. Stepwise evolution of

716 coral biomineralization revealed with genome-wide proteomics and transcriptomics.
717 PLoS One 11, e0156424.
718 Tambutté, S., Holcomb, M., Ferrier-Pagès, C., Reynaud, S., Tambutté, É., Zoccola, D.,
719 Allemand, D., 2011. Coral biomineralization: From the gene to the environment. J.
720 Exp. Mar. Bio. Ecol. 408, 58-78.
721 Thornton, D.J., Carlstedt, I., Sheehan, J.K., 1996. Identification of glycoproteins on
722 nitrocellulose membranes and gels. Mol. Biotechnol. 5, 171-176.
723 Watanabe, T., Suzuki, A., Minobe, S., Kawashima, T., Kameo, K., Minoshima, K., Aguilar,
724 Y.M., Wani, R., Kawahata, H., Sowa, K., Nagai, T., Kase, T., 2011. Permanent El Nino
725 during the Pliocene warm period not supported by coral evidence. Nature 471, 209-
726 211.
727 Weiner, S., Hood, L., 1975. Soluble protein of the organic matrix of mollusk shells: a potential
728 template for shell formation. Science 190, 987-989.
729 Wild, C., Woyt, H., Huettel, M., 2005. Influence of coral mucus on nutrient fluxes in
730 carbonate sands. Mar. Ecol. Prog. Ser. 287, 87-98.
731

Table 1. Quantification of AIMs and ASMs extracted from *P. australiensis* skeleton.

	AIM ($mg \cdot g^{-1}$)	ASM ($mg \cdot g^{-1}$)	Total organic matrix (% w/w)
2nd bleaching	1.31	0.12 ± 0.01	0.143
3rd bleaching	0.64	0.06 ± 0.01	0.07

732

733

Table 2. CHNS analysis of 3rd bleaching AIM.

	N (wt%)	C (wt%)	H (wt%)	S (wt%)
3bl AIM	1.42	21.63	3.15	1.05

734

735

736 # Figure Legends

737

738 **Figure 1. SEM images of *Porites australiensis* skeleton before and after second bleaching.**
739 (A) Surface of a skeleton fragment before the second bleaching. Fibrous structures of
740 microorganisms (red arrowheads) are visible. (B) The same skeleton surface of (A) after the
741 second bleaching. Contaminating fibers were completely removed. (C) Magnified image of
742 (A). (D) Magnified image of (B).

743

744 **Figure 2. SDS-PAGE of skeletal organic matrices.** (A) Silver staining, (B) Stains-all
745 staining, (C) Alcian blue staining. Twenty µl of sample solution was loaded in each lane for
746 silver staining and 15 µl for Stains-all staining and Alcian blue staining. ASM: Acid-soluble
747 matrix. LS-AIM: Laemmli-soluble acid-insoluble matrix. 2bl: second bleaching. 3bl: third
748 bleaching. MM: Molecular weight markers.

749

750 **Figure 3. FT-IR spectra of skeletal organic matrices.** Major peaks discussed in the main
751 text are colored. These signals indicate the presence of proteins or saccharides (i), lipids (ii),
752 sulphates (iii), phosphates (iv), and saccharides (v). ASM: Acid-soluble matrix. AIM: Acid-
753 insoluble matrix. 2bl: second bleaching. 3bl: third bleaching.

754

755 **Figure 4. SEM images of $CaCO_3$ crystal formed in the presence of *Porites* ASM.** (A-F)
756 Second bleaching ASM: $1\mu g \cdot mL^{-1}$ (A), $4\mu g \cdot mL^{-1}$ (B), $16\mu g \cdot mL^{-1}$ (C,D), $32\mu g \cdot mL^{-1}$ (E,F).
757 (G-I) Third bleaching ASM: $1\mu g \cdot mL^{-1}$ (G), $4\mu g \cdot mL^{-1}$ (H), $16\mu g \cdot mL^{-1}$ (I,J), $32\mu g \cdot mL^{-1}$ (K,L).
758 (M) $CaCO_3$ crystals generated in ASM-free solution. Morphology of the generated crystals
759 are affected by the presence of ASM in dose-dependent manner. The effect of third bleaching
760 ASM is more pronounced than that of second bleaching ASM.

761

762 **Figure 5. Monosaccharide composition of ASM and AIM after two (left) or three (right)**
763 **bleachings.** While the third bleaching did not produce any important change in the relative
764 percentages of monosaccharides in AIMS, it was more effective for ASMs, where it induced a
765 noticeable decrease of arabinose percentage.

766

767 **Figure 6. Enzyme-linked lectin assay (ELLA) on ASMs.** ELLA was performed with 21
768 lectins after the second (left) and third (right) bleaching steps. Absorbance values at 405 nm
769 were normalized to the highest value (DSL), corresponding to 100% reactivity (n = 3, means

770 ± S.D.).

771

772 **Figure 7. *In situ* localization of the DSL-reactive saccharide fraction.** Observation with
773 SEM in secondary electron (SE, A and H) and in back-scattered electron (BSE, B to G)
774 modes. A to F: positive control, with *Datura stramonium* lectin (DSL). G, H: negative control,
775 in the absence of DSL, but with gold-coupled anti-biotin. In (A) and (B), tips of needle-like
776 crystals point to the early mineralization zone (front side of the pictures). The early
777 mineralization zone is indicated in dotted circle in (C). Note that the gold particles,
778 characterized by tiny bright spots in BSE mode, are distributed evenly on the aragonite fibers.

779

780

781

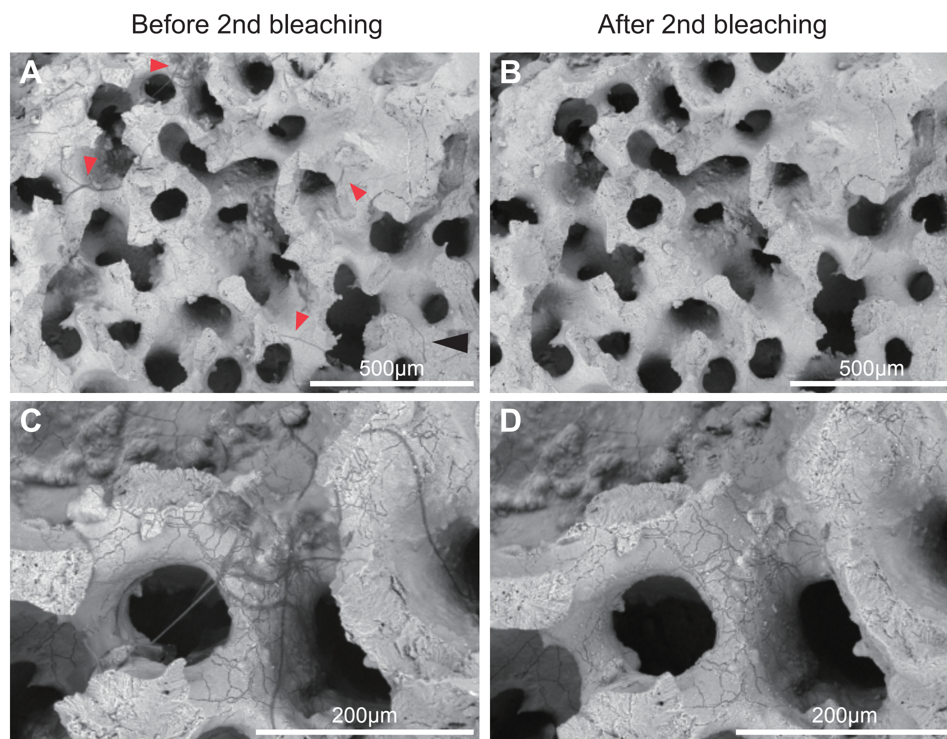

Figure 1.

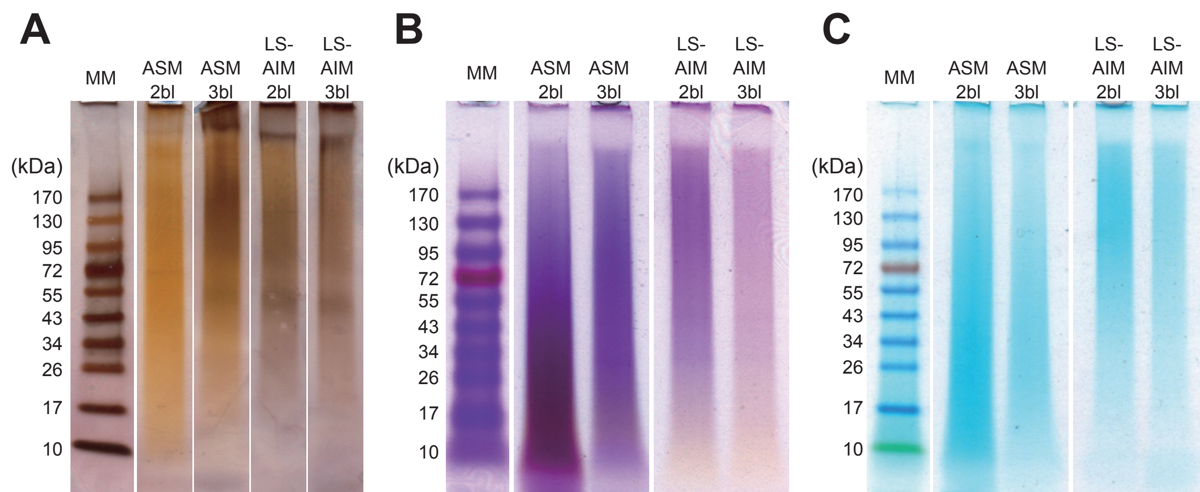

Figure 2.

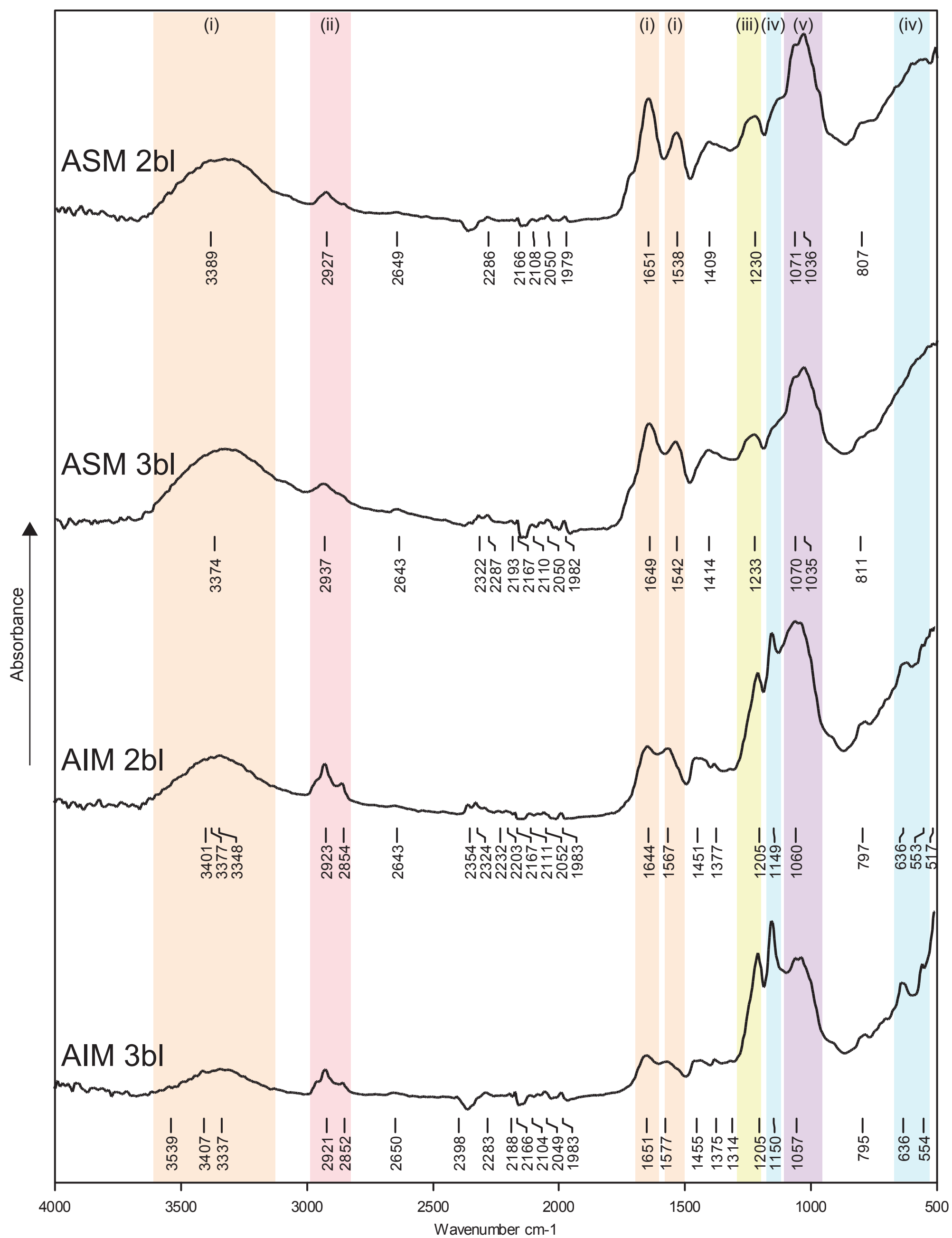

Figure 3.

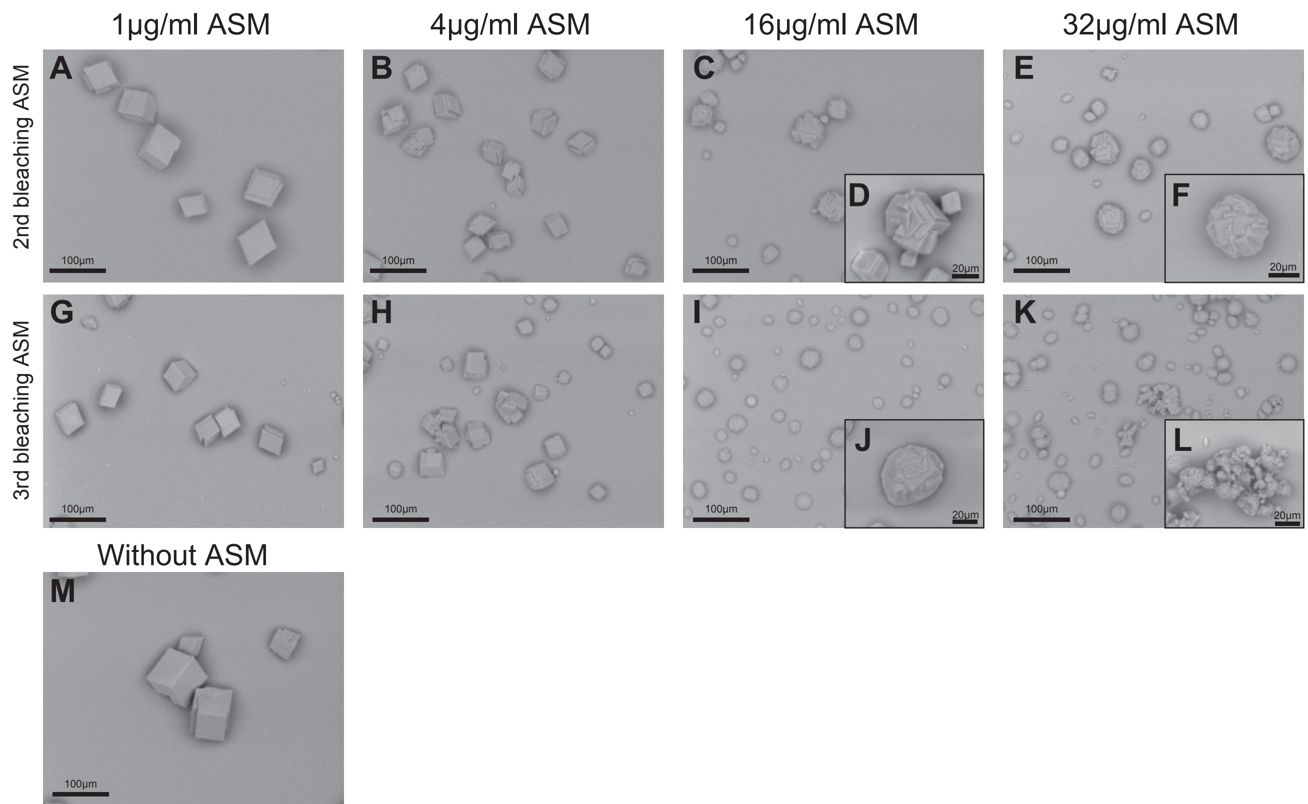

Figure 4.

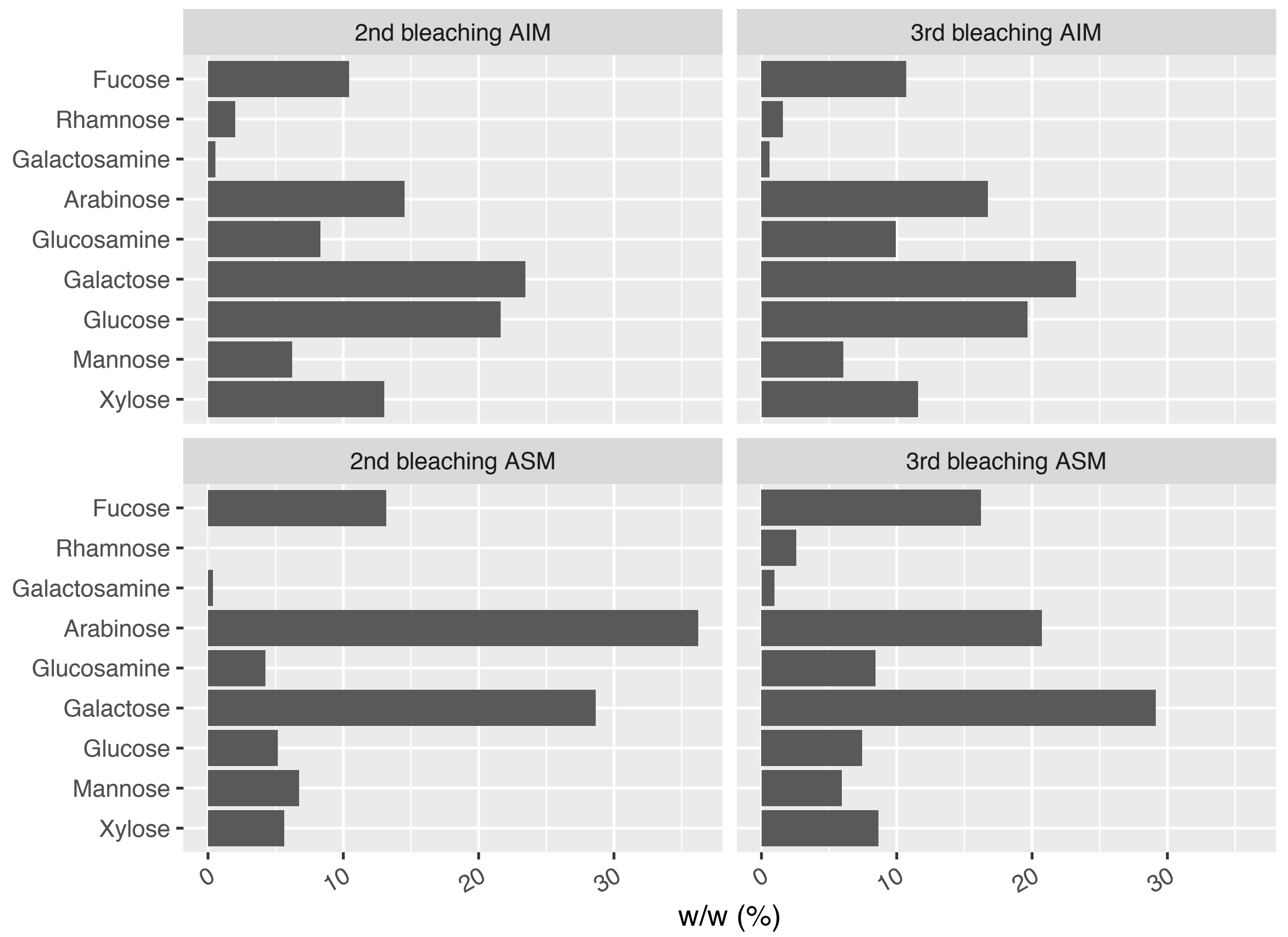

Figure 5.

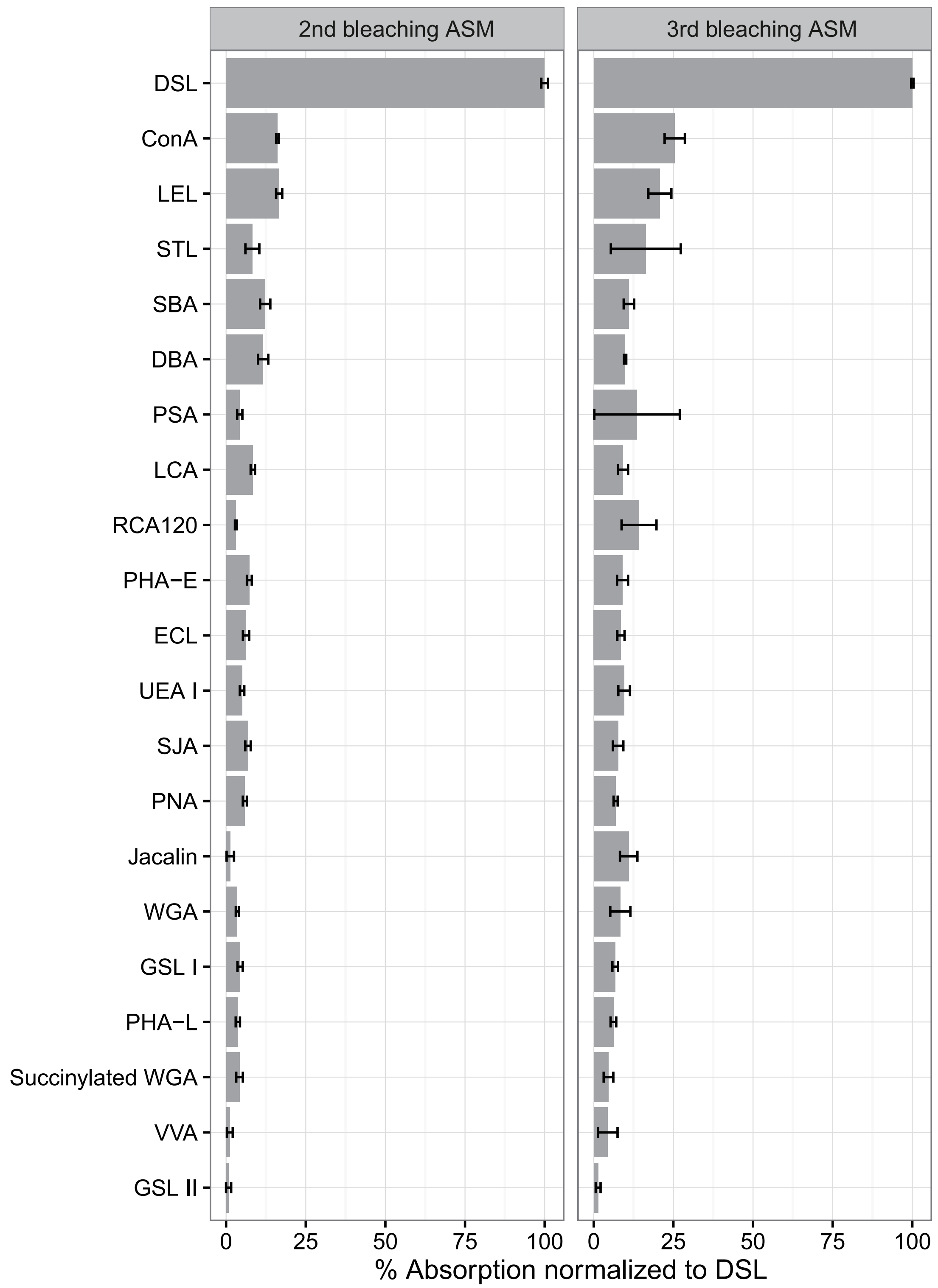

Figure 6.

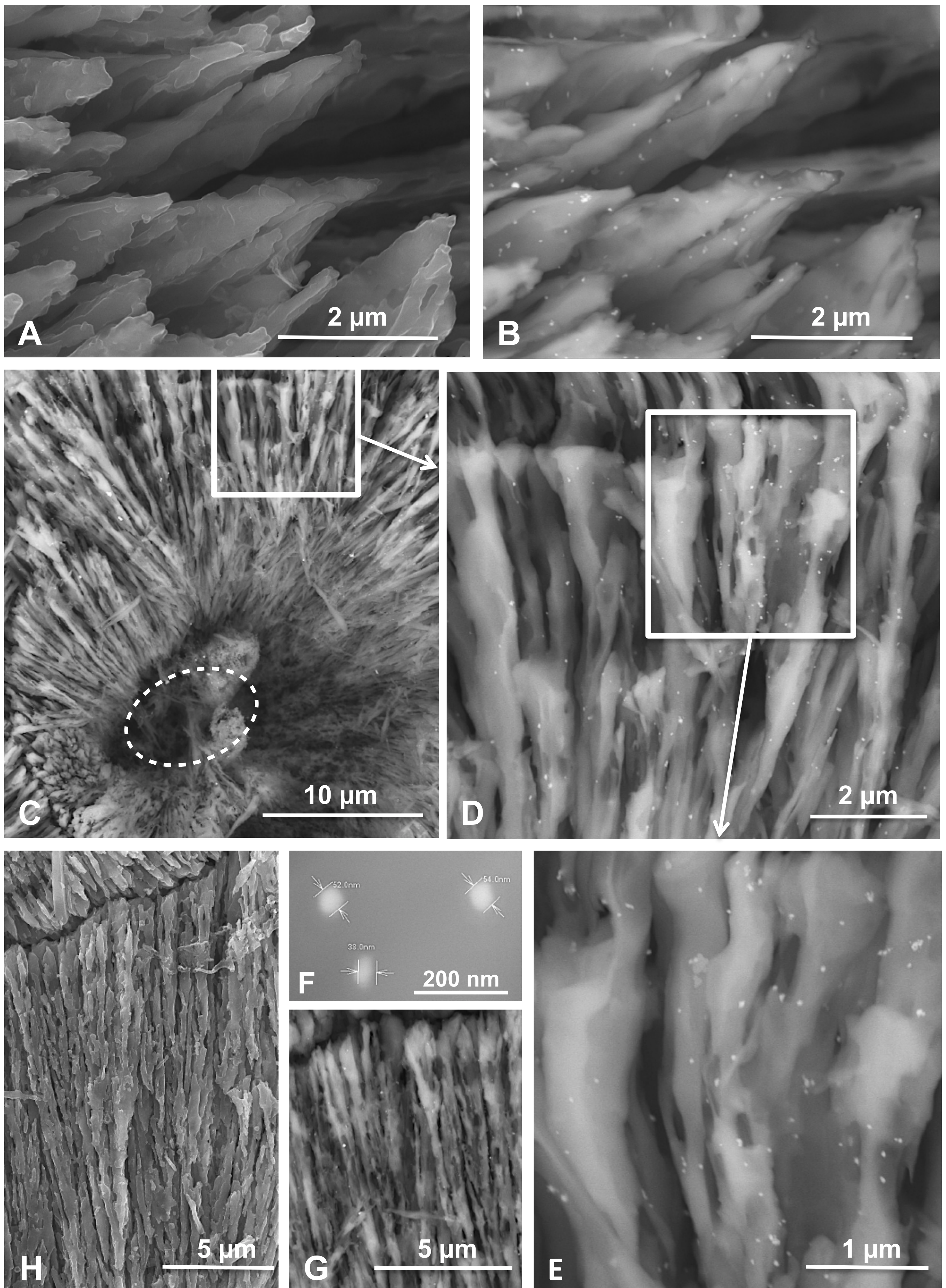

Figure 7.